

Combining Pixel- and Object-Based Machine Learning for Identification of Water-Body Types From Urban High-Resolution Remote-Sensing Imagery

Xin Huang, *Senior Member, IEEE*, Cong Xie, Xing Fang, and Liangpei Zhang, *Senior Member, IEEE*

Abstract—Water is one of the vital components for the ecological environment, which plays an important role in human survival and socioeconomic development. Water resources in urban areas are gradually decreasing due to the rapid urbanization, especially in developing countries. Therefore, the precise extraction and automatic identification of water bodies are of great significance and urgently required for urban planning. It should be noted that although some studies have been reported regarding the water-area extraction, to our knowledge, few papers concern the identification of urban water types (e.g., rivers, lakes, canals, and ponds). In this paper, a novel two-level machine-learning framework is proposed for identifying the water types from urban high-resolution remote-sensing images. The framework consists of two interpretation levels: 1) water bodies are extracted at the pixel level, where the water/shadow/vegetation indexes are considered and 2) water types are further identified at the object level, where a set of geometrical and textural features are used. Both levels employ machine learning for the image interpretation. The proposed framework is validated using the GeoEye-1 and WorldView-2 images, over two mega cities in China, i.e., Wuhan and Shenzhen, respectively. The experimental results show that the proposed method achieved satisfactory accuracies for both water extraction [95.4% (Shenzhen), 96.2% (Wuhan)], and water type classification [94.1% (Shenzhen), 95.9% (Wuhan)] in complex urban areas.

Index Terms—High resolution, machine learning, object-oriented, water detection, water extraction, water index.

I. INTRODUCTION

WATER is one of the most active and essential natural resources for the urban environments, which plays a crucial role in human life, social development, and climate change. However, water resources over urban areas are

Manuscript received September 30, 2014; revised March 27, 2015; accepted April 01, 2015. This work was supported in part by the National Natural Science Foundation of China under Grant 91338111 and in part by the Foundation for the Author of National Excellent Doctoral Dissertation of China under Grant 201348.

X. Huang, C. Xie, and L. Zhang are with the State Key Laboratory of Information Engineering in Surveying, Mapping and Remote Sensing, Wuhan University, Wuhan 430079, China (e-mail: xhuang@whu.edu.cn; xiecong@whu.edu.cn).

X. Fang is with the School of Geodesy and Geomatics, Wuhan University, Wuhan 430079, China.

Color versions of one or more of the figures in this paper are available online at <http://ieeexplore.ieee.org>.

Digital Object Identifier 10.1109/JSTARS.2015.2420713

gradually decreasing due to the rapid urbanization, population growth, agricultural irrigation, and environmental degradation [1], [2]. Therefore, it becomes an important task to retrieve and monitor the urban water information for management and decision-making of water resources in urban areas.

Remote sensing, as a convenient, rapid, effective, and timely Earth observation technique, can provide increasing possibilities for information extraction from urban water bodies. A number of papers have been published concerning water area extraction from remote-sensing data. In general, the methods can be divided into two groups: 1) spectral analysis, i.e., water information is retrieved by considering its radiometric characteristics in the multispectral bands and 2) image classification, i.e., feature extraction and classification techniques are employed for water-area detection and quantitative analysis. A literature review for the two groups is provided below.

A. Spectral Analysis

A notable example for the water spectral analysis is the normalized difference water index (NDWI) [3], which is computed using green and near-infrared (NIR) bands to enhance water features. However, NDWI cannot eliminate the disturbance of dark built-up areas, which are mixed with water bodies. To address this problem, modified NDWI (MNDWI) [4] was proposed by replacing the NIR band used in the NDWI with the shortwave infrared (SWIR) band to extract water surface while suppressing the noise from built-up areas. It should be noted that NDWI and MNDWI are not very appropriate for delineating water bodies from urban high-spatial resolution images since some urban structures (e.g., shadow, roads, and other dark objects) also have high response for the two indexes [5]. Feyisa *et al.* [6] developed a new automated water extraction index (AWEI), which can provide a fairly stable threshold value. In the experiments, AWEI achieved higher accuracies than the MNDWI and the maximum likelihood classification (MLC). Color space transformation has been also applied for delineating water bodies, such as HIS (hue, intensity, saturation) and HSV (hue, saturation, value) transformation. Jiang *et al.* [7] used indexes composition and the HIS transformation to separate water bodies from shadows. In the water bodies product of EU copernicus [8], the inland water was detected by applying thresholds to normalized difference vegetation index (NDVI),

NDWI, SWIR reflectance, and the hue component derived from the HSV transformation. Sun *et al.* [9] built a water-body extraction model based on the Munsell HSV transformation, trying to reduce the errors resulting from shadows. Nguyen [10] proposed a spectral pattern analysis for water-body extraction from Landsat 5 TM and SPOT 5 HRG images. It was found that the spectral pattern analysis was not only effective for detection of water bodies but also potential for indication of water quality.

B. Image Classification

Image classification based on feature extraction and machine learning is also an effective approach for water-area extraction from remote-sensing imagery. In [11], the K-means clustering as well as a series of processing chain, including edge detection, thresholding, and image erosion, was used to detect rivers from satellite images. Decision tree has been employed, according to the spectral characteristics of water bodies and other objects, to extract water surface from TM data [12]. The rule set method based on the object-oriented technique was used to extract water-body information from WorldView-2 image data, by combining spectral, geometric, and textural characteristics [13]. Adaboost algorithm [14], which was implemented by constructing a so-called “strong classifier” by training and integrating a set of “weak classifiers,” was used to improve the accuracy of water-body extraction. Zhou *et al.* [15] proposed an iterative method to extract urban water, through constructing segmented buffers with adaptive length and radius and introducing spatial consistency for gradually optimizing the classification. This method was proved as applicable in urban water extraction from high-resolution remote-sensing imagery.

On the other hand, image classification is also used for water extraction from SAR data. Mondal *et al.* [16] used the MLC for differentiating water areas from other areas from the TerraSAR-X image in a cloudy river valley region with a high classification accuracy score (94.92%) obtained. Klemenjak *et al.* [17] proposed an automatic method to extract river networks from high-resolution SAR data by using mathematical morphology and support vector machines (SVMs).

By summarizing the existing literature, it can be found that most of the papers concern the water-area extraction. However, to our knowledge, few studies refer to the identification of water-body types over urban areas, e.g., rivers, lakes, ponds, and canals. It should be noted that different water types have different effects for urban ecology and environments. Thus, it is necessary to identify the types of water when establishing the urban water geographical information database. On the other hand, in recent years, with the rapid development of the Earth observation techniques, a lot of high-resolution remotely sensed data become accessible and they are playing an important role in various urban-related applications. In this background, the availability of the high-resolution data makes it possible to further extract water-body types by considering the spatial and semantic information contained in the high-resolution images.

In the context, we propose a novel pixel-object two-level machine-learning model for identifying the water-body types from urban high-resolution optical satellite images. The main contributions of this paper lie in the following two aspects.

- 1) From the application point of view, extraction of the urban water types (e.g., rivers, lakes, ponds, and canals) from high-resolution images is investigated, which has been rarely studied in the existing literature.
- 2) From the methodology point of view, a novel pixel-object two-level machine-learning method is proposed, involving the water-area detection at the pixel level and the subsequent water-type classification at the object level.

This paper is organized as follows. Section II introduces the study areas (Wuhan and Shenzhen) as well as the high-resolution images used. Section III describes the proposed two-level machine-learning framework for identifying the urban water types. In Section IV, the proposed methodology is evaluated with experiments conducted on two high-resolution image datasets, and discussions and analysis for the results are made. Finally, discussions and conclusion are presented in Section V and Section VI, respectively.

II. STUDY AREAS AND DATASETS

Two typical mega cities of China, Shenzhen and Wuhan, are selected as the test sites in this study. Shenzhen is one of the several most-developed cities in China. However, its freshwater resources are very limited, and the ownership of water resources per capita for Shenzhen is only one-third of the national average. In general, Shenzhen is a city of shortage of water. The management and monitoring of water resources are therefore essential for the urban planning and decision-making. The other study site, Wuhan City, however, shows a quite different scenario. Wuhan is called the “city on rivers,” which is the largest inland port on the middle reaches of the Yangtze River. It has plentiful water resources with a number of various lakes, rivers, ponds, and canals. Its water surface area covers 25% of the whole city, and its gross amount of water resources ranks a high place in China.

In this study, two high-spatial resolution remote-sensing images are used for water detection and type classification: GeoEye-1 Wuhan and WorldView-2 Shenzhen. The images, as well as the corresponding ground truth references, are shown in Fig. 1. The detailed parameters of the two images are provided in Table I. The ground truth reference images were delineated manually from the high-resolution images by careful visual interpretation. A field campaign and the sufficient prior knowledge for the study sites can guarantee the reliability of the ground truth maps. In a typical Chinese city landscape, the water-body types refer to lakes, rivers, ponds, and canals, defined according to the official document from the Chinese National Administration of Surveying, Mapping and Geoinformation, within a project framework for the national geographic information monitoring [18]. The graphic examples for the four water types are illustrated in Fig. 2.

III. METHODOLOGY

The proposed pixel-object machine-learning framework for water extraction and classification is shown in Fig. 3. The water-area extraction is carried out at the pixel level, where a set

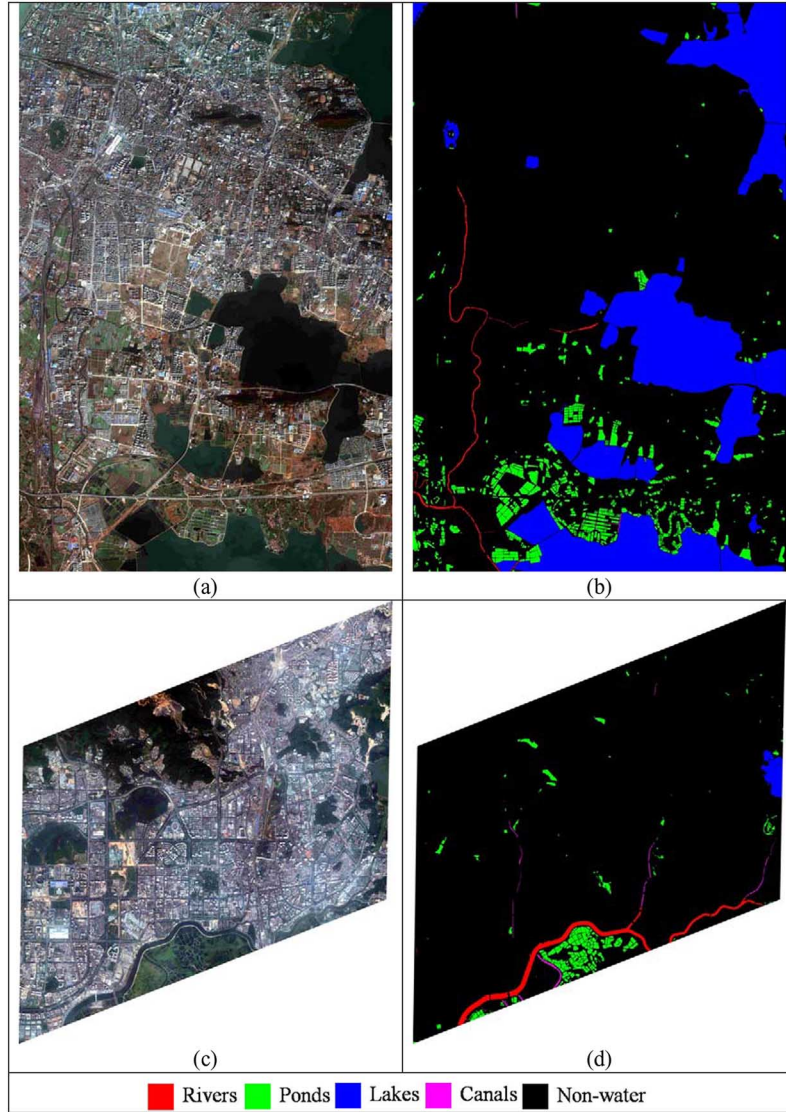


Fig. 1. (a) and (b) are GeoEye-1 Wuhan true-color image and ground truth reference, respectively; (c) and (d) are WorldView-2 Shenzhen true-color image and ground truth reference, respectively.

of information indexes are used for discriminating water bodies from other land-cover classes. The preliminary result for the water extraction is then input into the object level, such that the object-level information processing can focus on the water layer derived from the pixel level. The object-based processing chain includes image segmentation, textural and geometrical feature extraction, and machine learning for identifying various water types.

A. Pixel-Level for Water Extraction

The basic principle for the water extraction is that the water areas have large values on the NDWI, but very low response to the NDVI. However, a big challenge for water extraction from urban high-resolution imagery is that shadow and water have very low spectral reflectance in the visible and NIR bands. Thus, a recently developed morphological shadow index (MSI) [19] is utilized in this study for reducing the misclassification between water and shadow. The combination of the water,

shadow, and vegetation indexes makes it possible to effectively extract the water areas from urban high-resolution imagery. The information indexes considered are introduced as follows.

1) *Normalized Difference Water Index (NDWI)*: McFeeters [3] used the NDWI to delineate open-water features combining the green (Green) and NIR bands. It can be written as

$$NDWI = \frac{\text{Green} - \text{NIR}}{\text{Green} + \text{NIR}}. \quad (1)$$

2) *Normalized Difference Vegetation Index (NDVI)* [20]: NDVI is one of the most widely adopted vegetation indexes, according to the red radiation absorption and NIR reflectance of vegetation in the photosynthetic processes. NDVI is defined as the normalized ratio of the NIR band and red (Red) band

$$NDVI = \frac{\text{NIR} - \text{Red}}{\text{NIR} + \text{Red}}. \quad (2)$$

In this study, it can be also used to indicate the water information since water has relatively low NDVI values when there is no alga or vegetation on the water.

TABLE I
OVERVIEW OF GEOEYE-1 AND WORLDVIEW-2 DATASETS

	GeoEye-1	WorldView-2
Study area	Wuhan	Shenzhen
Acquisition date	December 21, 2009	November 03, 2010
Number of bands	4	8
Wavelength (nm)	Blue: 450–510 Green: 510–580 Red: 655–690 NIR: 780–920	Coastal: 400–450 Blue: 450–510 Green: 510–580 Yellow: 585–625 Red: 630–690 Red Edge: 705–745 NIR: 770–895 NIR2: 860–1040
Spatial resolution (m)	2.0	2.0
Image size (pixel)	6327×4156	6433×5409
Sun angle azimuth (°)	162.9	159.6
Sun angle elevation (°)	34.1	50.4
Off nadir view angle (°)	21.8	17.6
Cloud cover (%)	0	0

3) *Morphological Shadow Index (MSI)* [19]: MSI is a recently developed urban shadow index, which is able to automatically extract shadow from urban high-resolution imagery. It is constructed by describing the spectral–spatial properties of shadow using a series of morphological operations. The basic principle is that shadow areas as well as the spatially adjacent buildings will produce a large local contrast. It is a dual operator of the morphological building index (MBI) [21]. Buildings and shadow correspond to the bright and dark components, respectively, and hence, they are represented using white and black top-hat transform for the MBI and MSI. MSI can be calculated by

$$MSI = \frac{\sum_{d,s} DMP_{BTH}(d, s)}{D \times S} \quad (3)$$

where d and s indicate the direction and length of a linear structuring element (SE), respectively; D and S are the number of directions and scales for the differential morphological profiles (DMP_{BTH}), respectively. MSI is defined as the mean of the DMP_{BTH} profiles since shadow shows large local contrast compared to the neighborhoods in various scales and directions. Consequently, shadow areas have large MSI feature values. Readers can refer to [19] and [21] for details about MBI and MSI.

Combination of the aforementioned information indexes (NDWI, NDVI, and MSI) makes it possible to effectively extract water areas from urban high-resolution images. A graphic example is demonstrated in Fig. 4, where (a) shows an urban lake landscape. A major difficulty for extracting water surface from urban images is to remove shadow, especially for the high-resolution images. To this aim, the NDWI [Fig. 4(b)], NDVI [Fig. 4(c)], and MSI [Fig. 4(d)] are used to highlight the water, vegetation, and shadow, respectively, and to enlarge the difference between water and other urban structures. In Fig. 4(d), it can be seen that the MSI is able to indicate the shadow from both buildings and trees. With these information indexes, the water, shadow, and vegetation can be conveniently extracted by manually setting a set of thresholds (i.e., 0.24 for NDWI, 0.09 for NDVI, and 0 for MSI) [Fig. 4(e)].

In this study, in order to sufficiently exploit the information indexes for urban water extraction, a set of machine-learning algorithms are employed to interpret these indexes. The machine-learning algorithms considered include both state-of-the-art and newly proposed ones, which are briefly described in Section III-C. Subsequently, the result obtained by the machine learning at the pixel level is used as the preliminary water layer and input into the object level for further identifying the water-body types.

B. Object Level for Identification of Water-Body Types

Although the combination of the water, vegetation, and shadow indexes can effectively extract water surface, it may fail to discriminate between various water types. This phenomenon can be clearly observed in Fig. 5, where the feature values of the NDWI, NDVI, and MSI for different water types are highly overlapped. This observation can also be supported by the Jeffreys–Matusita (J–M) distance [22], which is used to quantify the degree of the overlap among different types of water bodies, as shown in the Table II. J–M distance is a widely used quantitative measure of the separability between two classes, ranging from 0 to 2. A high value indicates a better separability. From the table, it can be seen that it is very difficult to discriminate between various kinds of water areas by only considering the NDVI, NDWI, and MSI features at the pixel level, since the J–M values are very low. Consequently, we propose to consider the geometrical and textural attributes of each water body at the object level for the type identification. The proposed processing flow includes the following steps.

Step 1) *Segmentation*: The water areas extracted from the pixel level (i.e., the preliminary result) are used to generate a set of water segments. The segmentation can be simply carried out by a region-growing method, where the water pixels derived from the preliminary result are viewed as seed points and the neighboring water pixels are gradually included into the segment.

Step 2) *Feature extraction*: The object-based features considered in this study refer to:

- a) Area: It indicates the number of the pixels constituting the image object. In an urban image, the lakes and rivers always have large area values.
- b) Shape index: It is defined as the border length of an image object divided by four times the square root of its area. It can also be understood as the ratio between the border length of an object and the perimeter of the square with the same area. It describes the smoothness of an image-object border

$$S = \frac{B}{4\sqrt{A}} \quad (4)$$

where B is the border length of the image object, and A indicates the area of the object.

- c) Density: It can be calculated as the ratio of the object's total number of pixels to its


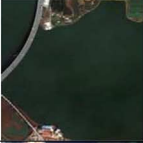










	Rivers	Lakes	Canals	Ponds
Wuhan GeoEye-1				
Shenzhen WorldView-2				
Ground sampling				
Characteristics (Keywords)	* Surface runoff * Affluent * Meanders	* Large area * Water supply * Landscape	* Artificial * Irrigation * Narrow	* Small area * Aquatic plants * Fish-farming

Fig. 2. Graphic examples for the four water types: rivers, ponds, lakes, and canals, as well as the ground sampling and the key words for their characteristics.

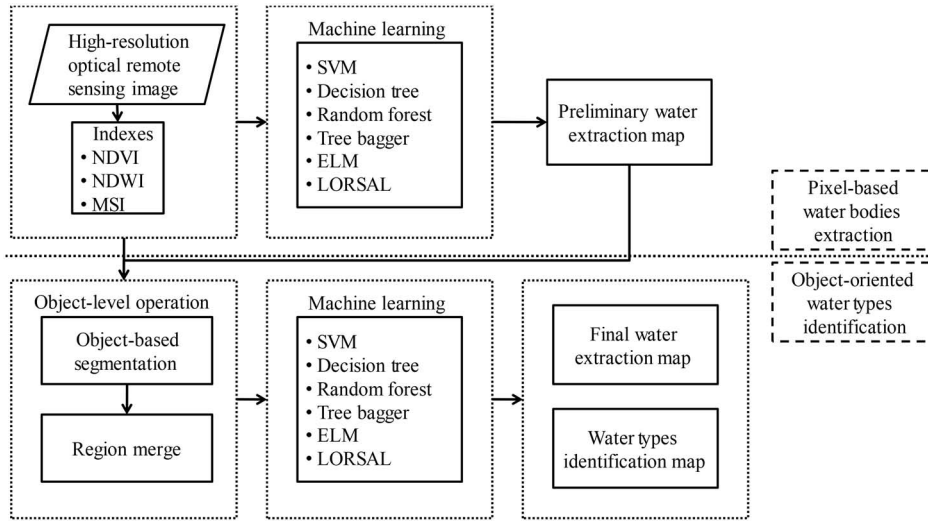


Fig. 3. Proposed water-body extraction and type classification framework.

approximated radius. It helps to delineate the compactness of an object, i.e., the object has large density if its shape is close to a regular square. An elongated structure corresponds to small-density value. The formula of the density can be written as

$$D = \frac{\sqrt{A}}{1 + \sqrt{Var(X) + Var(Y)}} \quad (5)$$

where A is the number of pixels forming the image object, and $Var(X)$ and $Var(Y)$ indicate the variance of X and Y coordinates of all pixels that constitute the object, respectively.

- d) Length-to-width ratio: It represents the ratio of the length and width of the bounding box for an image object. Usually, the length-to-width ratio of canals is higher than lakes and ponds on account of their straight and narrow shape.

- e) Homogeneity: The homogeneity, derived from the gray-level cooccurrence matrix (GLCM) [23], is used to describe the textural feature of an object. It is considered in this study since the texture of water bodies is often more homogeneous than shadow.

A series of statistics derived from the samples of GeoEye-1 Wuhan test site are shown in Fig. 6, where the distributions of the feature values at the object level accord well with the previous analysis. A satisfactory separability between various types of water bodies is obtained at the object level. Please note that besides the four water types, shadow objects are considered, since the residual shadow that was misclassified as water at the pixel level can be corrected by the object-based features. It is a merit of the proposed two-level pixel-object framework.

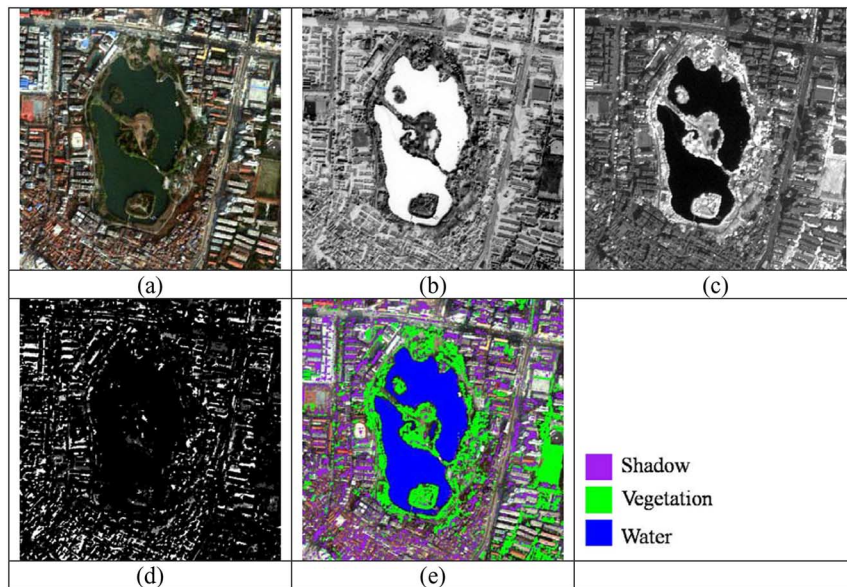


Fig. 4. Example showing urban water-body extraction based on NDWI, NDVI, and MSI. (a) Example image. (b), (c), and (d) Shows the NDWI, NDVI, and MSI feature images, respectively. (e) Water extraction result derived from the information indexes based on a set of manually selected threshold values.

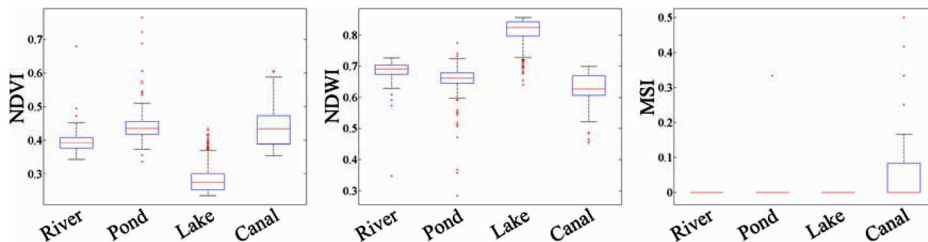


Fig. 5. Statistics of the information indexes for the four water types. Each box plot shows the location of the 25, 50, and 75 percentiles using horizontal lines. The two whiskers cover the 99.3 percentile of the data, and the red “+” is the outlier outside the two whiskers. The plots are based on the statistics of the samples derived from the GeoEye-1 Wuhan test site.

TABLE II
J–M DISTANCE BETWEEN DIFFERENT WATER TYPES USING NDVI,
NDWI, AND MSI

	Ponds	Lakes	Canals
Rivers	0.241	0.443	1.045
Ponds	–	0.568	0.543
Lakes	–	–	0.724

Step 3) *Machine learning for classification of water types:*

A set of machine-learning methods are employed to interpret the object-based textural and geometrical features for identifying the type of each water object. At the object level, the water segments are classified into four types (rivers, lakes, ponds, and canals) as well as the shadow areas, since some shadow pixels that were wrongly identified as water are also input into the object level. As aforementioned, the false alarms of the shadow can be further suppressed by taking the geometrical features into account at the object level.

Step 4) *Outputs:* Based on the feature extraction and machine learning, the refined water bodies as well as their types can be obtained as the final products.

C. Machine Learning

The machine-learning methods play an important part in this study, for the preliminary water extraction at the pixel level and the further water-type identification at the object level. It should be noted that the motivation of this paper is not to investigate the performance of the machine-learning algorithms, but to construct a novel pixel-object two-level machine-learning framework, with due consideration of the requirements for water-area extraction and the water-type classification. The machine-learning methods considered in this paper refer to a series of state-of-the-art algorithms, some of which are recently developed for remote-sensing image classification. A brief description is given below.

1) *Support Vector Machine (SVM):* SVM is a popular machine-learning algorithm based on the statistical learning theory and the structural risk minimization (SRM) principle [24]. SVM has a high generalization performance and is suitable for the image classification with high dimension feature space and small training sample set [25].

2) *Extreme Learning Machine (ELM):* ELM is a single-hidden layer feedforward neural network (SLFN), which is a fast and effective machine-learning method with high generalization performance [26]. In contrast to other learning

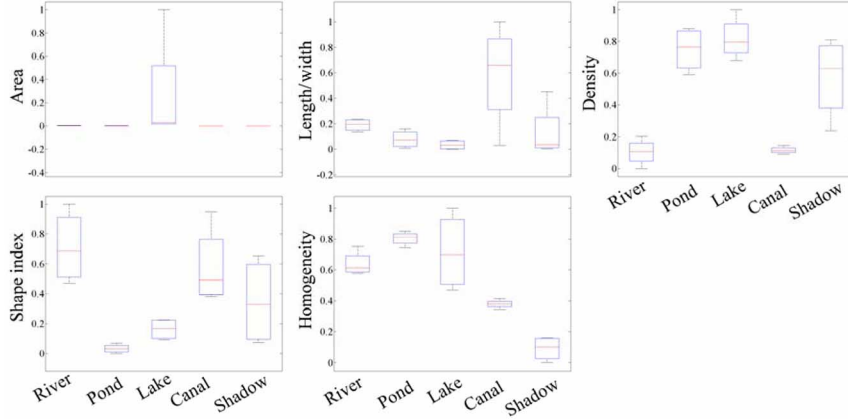


Fig. 6. Feature distributions of the four water types at the object level. Each box plot shows the location of the 25, 50, and 75 percentiles using horizontal lines. The two whiskers cover the 99.3 percentile of the data, and the red ‘+’ is the outlier outside the two whiskers. The plots are based on the statistics of the samples selected from the GeoEye-1 Wuhan test site, where 8, 17, 6, 3, and 11 objects for rivers, ponds, lakes, canals, and shadow, respectively, are considered.

algorithms, an advantage of the ELM is that it does not need extra parameters and it is not time-consuming. ELM is a relatively new classifier and has been introduced for processing remote-sensing images very recently [27].

3) *Decision Tree*: Decision tree is one of the most commonly used machine-learning methods for supervised classification [28], [29], which is composed of a series of interior nodes and leaf nodes, corresponding to the input and target variables, respectively. Many decision-tree algorithms have been developed for data mining, such as ID3 [30], C4.5 [31], and CART [32].

4) *Random Forest (RF)*: RF is an ensemble machine-learning method based on the principle that a subset of variables are selected randomly to construct a collection of decision trees and the output of the trees with the most votes is regarded as the result. It is able to improve the prediction accuracy of a simple decision-tree [33].

5) *Tree Bagger (TB)* [34]: The principle of the TB is very similar to the RF. It also creates an ensemble of bagged decision trees, but without the selection of a random subset of the features for each tree compared to the RF.

6) *Logistic Regression via Variable Splitting and Augmented Lagrangian (LORSAL)*: LORSAL is a recently introduced classification algorithm [35], and it has been successfully applied to the hyperspectral image classification [36]. Its basic principle is to learn the class posterior probability distributions using a multinomial logistic regression (MLR) model [37]. LORSAL has the advantage of dealing with the large datasets with multiple features, which accords well with the case in this study.

IV. EXPERIMENTS AND ANALYSIS

A. Parameter Setting

The parameters for both pixel and object levels in the experiments are provided below.

1) *Pixel Level: Feature extraction*: The scale parameters for the MSI are set to $S_{\min} = 3$ and $S_{\max} = 15$ with the interval $\Delta s = 3$. $S_{\min} = 3$ and $S_{\max} = 15$ are determined according

TABLE III
MEAN AND STANDARD DEVIATION OF THE KAPPA COEFFICIENT OF THE WATER EXTRACTION FOR GEOEYE-1 WUHAN DATASET

Method	Mean	Standard deviation
Linear-SVM	0.930	0.004
RBF-SVM	0.941	0.004
C4.5	0.918	0.014
CART	0.876	0.021
TB	0.927	0.006
RF	0.926	0.005
ELM	0.854	0.028
LORSAL	0.921	0.008

to the minimal and maximum dimension of a shadow, respectively, by considering the spatial resolution of the images. Δs is set to 3, following our previous studies [19], [21].

Machine learning: The number of the training samples of water and nonwater is set to 1000 pixels, respectively, generated randomly for ten times from the ground truth references. A five-fold cross-validation is used to seek the optimal parameters. The mean and standard deviation of the Kappa coefficients are reported as the water detection and classification accuracy. The parameter setting for various machine-learning methods is summarized as follows.

- 1) SVM is run with both linear and RBF kernels. For the RBF kernel, the ranges for optimization of the RBF kernel width and the penalty coefficient are (0.0001, 0.001, 0.01, 0.1, 1, 10) and (0.1, 1, 10, 100, 500, 1000), respectively.
- 2) The parameter of RF mainly refers to the number of trees. In this study, a set of values (10, 20, 50, 100, 500, 1000) is defined for parameter selection.
- 3) The key parameter for the ELM is the number of neurons in the hidden layer. Its range for the parameter selection is (10, 20, 50, 100, 500, 1000).
- 4) The LORSAL classifier refers to the sparseness parameter lambda. The optimal value is selected from (0.001 0.01 0.1 1 10 50).

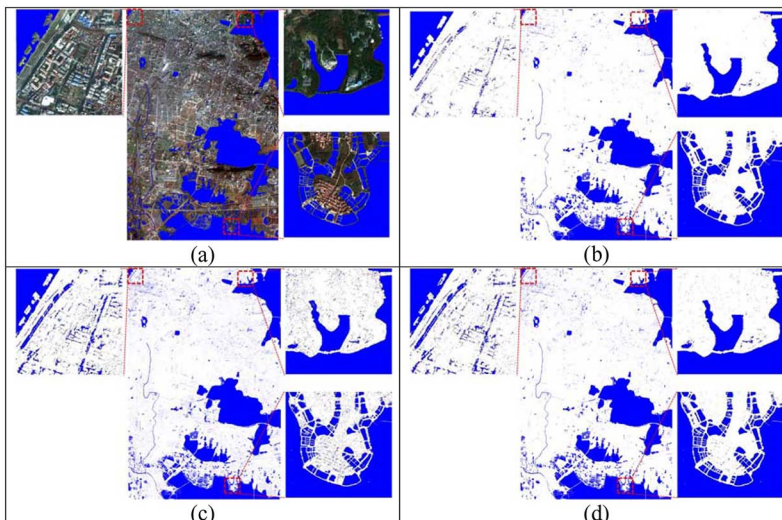


Fig. 7. Results of water extraction for GeoEye-1 Wuhan dataset: (a) ground truth; (b) RBF-SVM; (c) CART; and (d) RF.

TABLE IV
ACCURACIES OF WATER-TYPE IDENTIFICATION FOR GEOEYE-1 WUHAN DATASET

Method	Kappa	F-measure			
		Rivers	Ponds	Lakes	Canals
Linear-SVM	0.946	0.624	0.791	0.989	0.417
RBF-SVM	0.655	0.289	0.254	0.595	0.516
C4.5	0.950	0.633	0.811	0.989	0.223
CART	0.959	0.769	0.843	0.989	0.352
TB	0.957	0.782	0.830	0.986	0.693
RF	0.954	0.775	0.818	0.983	0.682
ELM	0.879	0.679	0.639	0.911	0.367
LORSAL	0.798	NA	0.631	0.826	NA

NA, not available.

2) *Object Level: Feature extraction:* There are no free parameters for the object-based feature extraction.

Machine learning: Please note that the training samples used in this stage are based on objects rather than pixels. In this regard, the number of the training samples is quite limited, especially when only considering the objects of water. Thus, the cross-validation strategy is not used at the object level, and the final results are reported with the optimal parameters that achieve the best classification for the water-type classification.

B. Results for the GeoEye-1 Wuhan

1) *Water Extraction (Pixel Level):* The accuracies for the water extraction are provided in Table III, where the training samples were randomly selected from the reference by ten times, and the mean and standard deviation of the Kappa coefficient are recorded for accuracy assessment. The Kappa coefficient is employed since it is insensitive to the imbalance for the number of pixels between the water and nonwater classes.

From the table, it can be seen that SVM outperformed other machine-learning methods in terms of the accuracy of the water

TABLE V
MEAN AND STANDARD DEVIATION OF THE KAPPA COEFFICIENTS OF THE WATER EXTRACTION FOR WORDVIEW-2 SHENZHEN DATASET

Method	Kappa	
	Mean	Standard deviation
Linear-SVM	0.678	0.022
RBF-SVM	0.690	0.049
C4.5	0.543	0.086
CART	0.545	0.045
TB	0.681	0.015
RF	0.661	0.027
ELM	0.500	0.051
LORSAL	0.657	0.031

extraction. In addition, RBF-SVM achieves the highest value of the Kappa with the lowest standard deviation, which shows its stability for the classification. It can be noted that the RF and the TB also yield satisfactory results, which are slightly lower than the SVM. The CART and ELM seem to be unsuitable for water extraction in the pixel level since they give relatively small Kappa score and high standard deviation.

Some maps for the water-area extraction are shown in Fig. 7 as a visual inspection. In order to show the details of the results, three local areas are selected for comparison of three machine-learning methods: RBF-SVM [Fig. 7(b)], CART [Fig. 7(c)], and RF [Fig. 7(d)]. By comparing the results of the machine-learning methods and the ground truth, it can be found that most of the misclassifications are related to the urban shadow. In particular, the CART method is subject to more false alarms for shadow, and its result shows pepper-and-salt effect, which is not observed in the RBF-SVM and RF.

2) *Water-Type Classification (Object Level):* The accuracy scores for the water-type identification are provided in Table IV. Please note that the classification experiment will not be generated multiple times by randomly selecting the training samples, since the number of the object-based training samples is very limited for each water class. In this case, the number of the

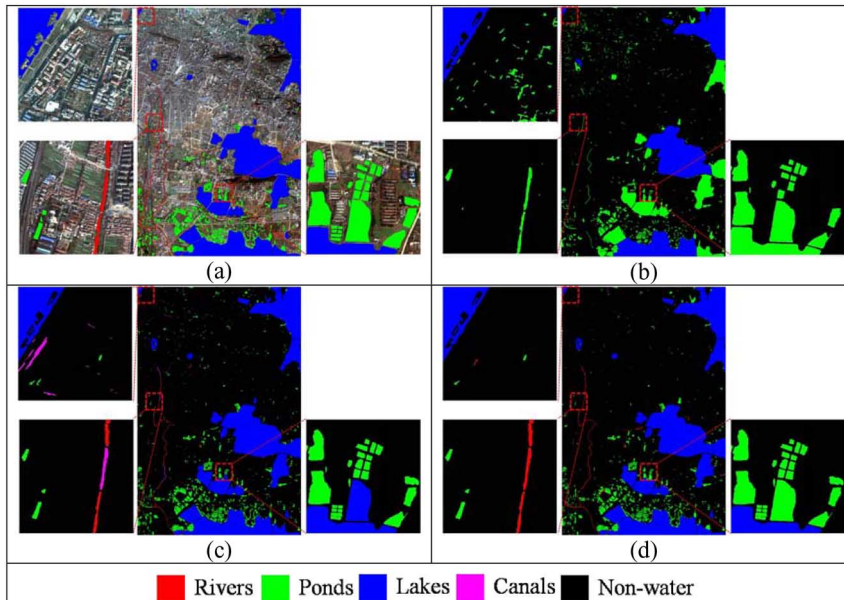


Fig. 8. Results of water-type identification for GeoEye-1 Wuhan dataset: (a) ground truth; (b) RBF-SVM; (c) C4.5; and (d) RF.

training samples (in objects) is 8, 17, 6, 3, and 11 for rivers, ponds, lakes, canals, and shadow, respectively. With respect to the accuracy assessment, in addition to the Kappa coefficient, *F-measure* [38] is also used for accuracy assessment. *F-measure* is a combination of the producer's and user's accuracy (PA and UA), i.e., a balance between the omission and commission errors. It is defined as

$$F\text{-measure} = \frac{(1 + \beta^2) * PA * UA}{\beta^2 * PA + UA} \quad (6)$$

with $\beta = 1$ in this paper.

Table V shows interesting results. In general, the decision-tree methods (including C4.5, CART, TB, and RF) as well as the linear-SVM achieve satisfactory accuracies in terms of the Kappa coefficients, outperforming the complicated machine-learning algorithms, e.g., nonlinear SVM, ELM, and LORSAL. It reveals that the object-based geometrical and textural features are adequate for identifying different water types. A simple combination, e.g., a decision-tree or linear decision, is therefore effective for the classification. This phenomenon can be supported by the statistics in Fig. 6, where the object-based features we selected are able to discriminate between different water types. In this case, the nonlinear learning (RBF-SVM), multilevel neural network (ELM), and sparse representation (LORSAL) may lead to overfitting of the classification and make the classification problem complicated.

Some classification maps are shown in Fig. 8 for a visual inspection. It can be seen that the result of the RBF-SVM is not satisfactory with many misclassifications observed [Fig. 8(b)]. By comparing Fig. 8(c) and (d), it can be found that some small errors between ponds and lakes occur in the C4.5, but do not exist for the RF. Similar phenomenon can also be observed between canals and rivers, which are wrongly classified by the C4.5 but are correct for the RF. These observations are consistent with the class-specific accuracies in Table VI, where the

TABLE VI
ACCURACIES OF WATER-TYPE IDENTIFICATION FOR WORLDVIEW-2
SHENZHEN DATASET

Method	Kappa	F-measure			
		Rivers	Ponds	Lakes	Canals
Linear-SVM	0.849	0.798	0.707	0.939	0.414
RBF-SVM	0.837	0.889	0.715	0.939	0.546
C4.5	0.900	0.880	0.914	0.630	0.561
CART	0.815	0.621	0.923	NA	0.289
TB	0.941	0.971	0.917	0.939	0.775
RF	0.939	0.965	0.914	0.939	0.775
ELM	0.706	0.587	0.537	0.486	0.346
LORSAL	0.774	0.909	0.787	NA	NA

classification accuracies of various water types achieved by RF are among the best.

C. Results for the WorldView-2 Shenzhen

1) *Water Extraction (Pixel Level)*: The accuracies of water extraction for the WorldView-2 Shenzhen dataset are provided in Table V. Generally speaking, the water extraction accuracies in Shenzhen are much lower than Wuhan, which can be attributed to the fact that the amount of the shadow in the WorldView-2 Shenzhen image is more than Wuhan, since most of the study area for Shenzhen is in the city center, while the Wuhan test image covers a lot of rural areas and urban fringes. Therefore, a large number of misclassifications exist between water and shadow in the Shenzhen dataset (Fig. 9), which significantly reduce the water extraction accuracy. However, the performance for the machine-learning methods is similar to the Wuhan experiment. The SVM methods, as well as the RF and TB, achieve relatively satisfactory results.

Some maps of water-body extraction are presented in Fig. 9 for a visual comparison. It can be seen that the high accuracy of the water detection obtained by the SVM and RF is

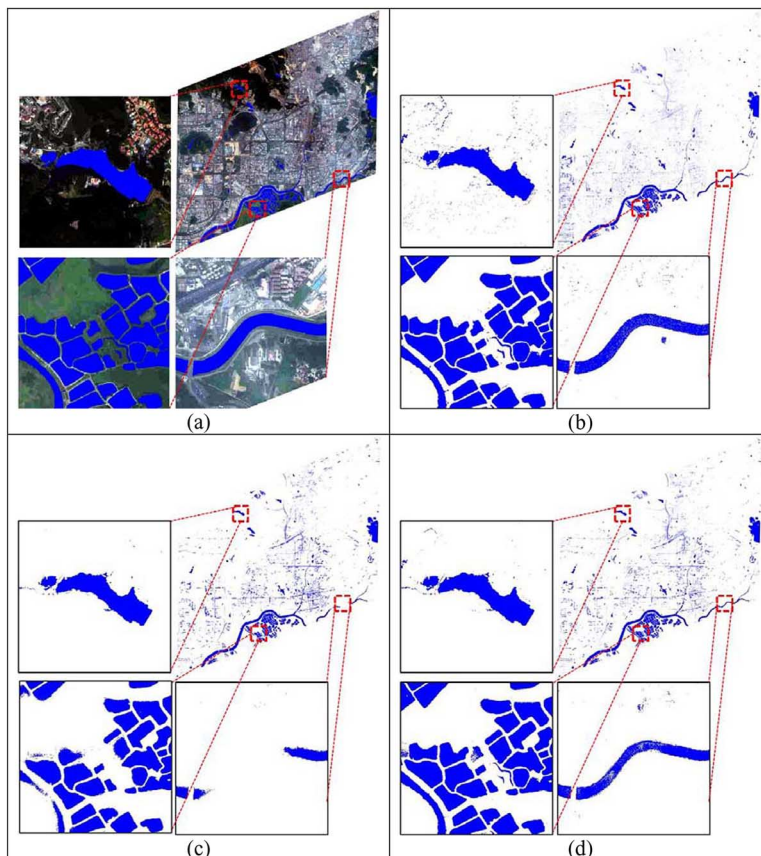


Fig. 9. Results of water-body extraction for WorldView-2 Shenzhen dataset: (a) ground truth; (b) RBF-SVM; (c) C4.5; and (d) RF.

consistent with their visual results, where the false alarms and misclassifications are smaller than other methods.

2) *Water-Type Identification (Object Level)*: The accuracies of water body-type identification for WorldView-2 Shenzhen dataset are presented in Table VI. The number of training samples in objects is 5, 13, 2, 8, and 19 for rivers, ponds, lakes, canals, and shadow, respectively. The performances of the machine-learning methods show similar conclusions to the Wuhan test site. The decision-tree algorithms achieve significantly higher water classification accuracies compared to SVM, ELM, and LORSAL. In particular, the RF and TB give the optimal results in terms of both Kappa coefficients and class-specific accuracies (F-measure scores). In this study area, in general, the decision-tree methods also outperform kernel learning (RBF-SVM), neural networks (ELM), and the sparse classifier (LORSAL). It is revealed that the decision-tree classifiers are more suitable for the object-based water-type classification than other machine-learning methods, which have more complicated decision rules.

Some classification maps of water-type classification are presented in Fig. 10 for a visual inspection. It can be observed that the RF method indeed provides more accurate water-type classification, as the examples shown in the figure.

V. DISCUSSIONS

In this section, some important issues related to the proposed two-level pixel-object framework for water extraction and water-type classification are discussed.

The influence for the number of training samples is discussed for the water-detection experiment. Fig. 11 shows the relationship between the accuracy (average Kappa values and standard deviation) and the processing time (s), with different sizes of training samples. It can be seen that increasing the number of training samples can lead to higher accuracy scores with lower standard deviation, but, at the same time, its computation time also increases. Specifically, 100, 200, 400, 800, 1000, and 2000 samples (in pixels) per class (i.e., water and nonwater) are considered, and the average Kappa coefficient and the standard deviation are reported in Fig. 12 for various machine-learning methods. It can be seen that the trend is similar to the results shown in Tables III and V, where 1000 pixels per class were used for training. The SVM classifiers, both linear and kernel-based, as well as the TB and RF are among the most accurate ones, regardless of the number of training samples. The influence of the number of training samples at the object level is not discussed here since the available number of samples at the object level is much smaller than the pixel level.

Another interesting phenomenon for the proposed framework is the difference of the water-detection accuracy between pixel and object levels (Fig. 13). It can be clearly seen that, in most cases, the accuracy of the water extraction at the pixel level has been significantly improved by the object-level processing. It is not surprising since a series of object-based geometrical and textural features are further utilized to remove the false alarms of shadow. It is implied that an accurate water extraction from remotely sensed imagery, especially for the

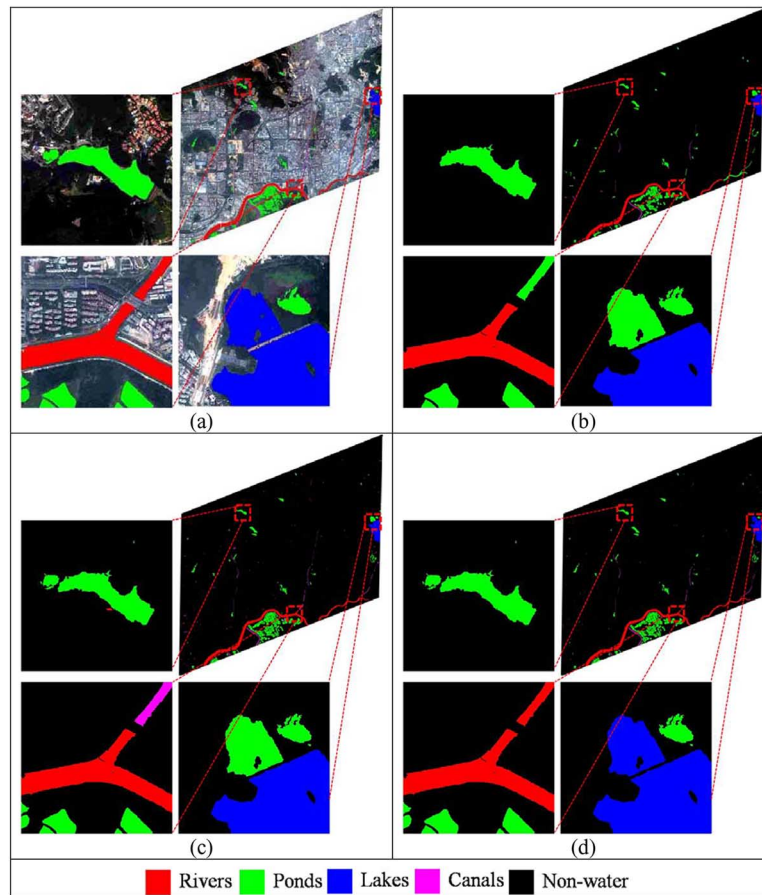


Fig. 10. Results of water body-type identification for WorldView-2 Shenzhen dataset: (a) ground truth; (b) RBF-SVM; (c) C4.5; and (d) RF.

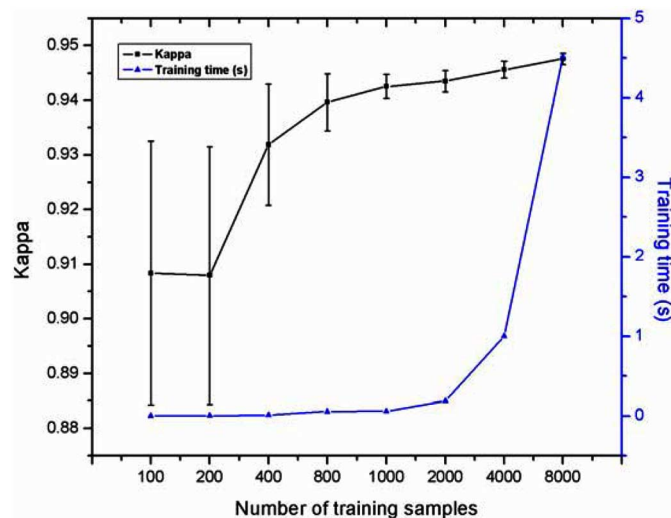


Fig. 11. Accuracy scores (average Kappa value and standard deviation) and the training time with different number of training samples.

high-resolution data, should be relied on both spectral and spatial information.

At the pixel level, both NDVI and NDWI have been utilized to delineate preliminary water map. Fig. 14 illustrates the scatter plot of NDVI and NDWI, where 1000 samples per class (i.e., water and nonwater) are considered. It can be seen that an individual index can separate water and nonwater to

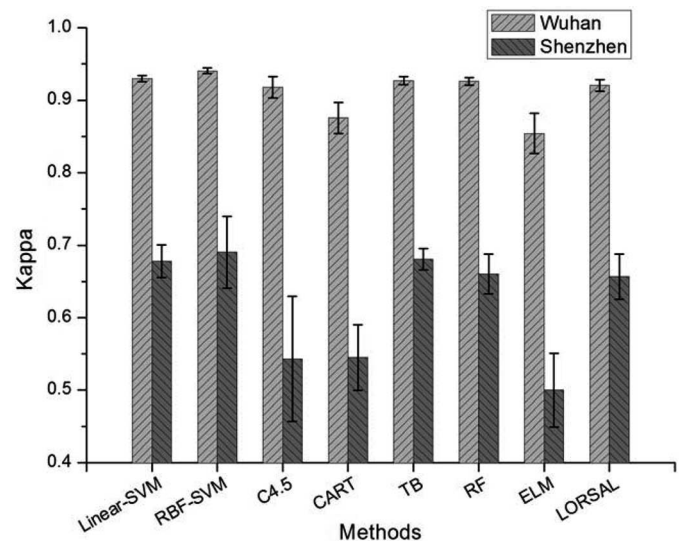


Fig. 12. Average and standard deviation of the accuracies for water detection for GeoEye-1 Wuhan and WorldView-2 Shenzhen datasets when different training samples are used for machine learning.

some degree, and combination of NDVI and NDWI can slightly facilitate the extraction of water areas. In reality, there is information redundancy in using both NDVI and NDWI due to a high correlation between them. Hence, it is not essential to include both indexes in water extraction.

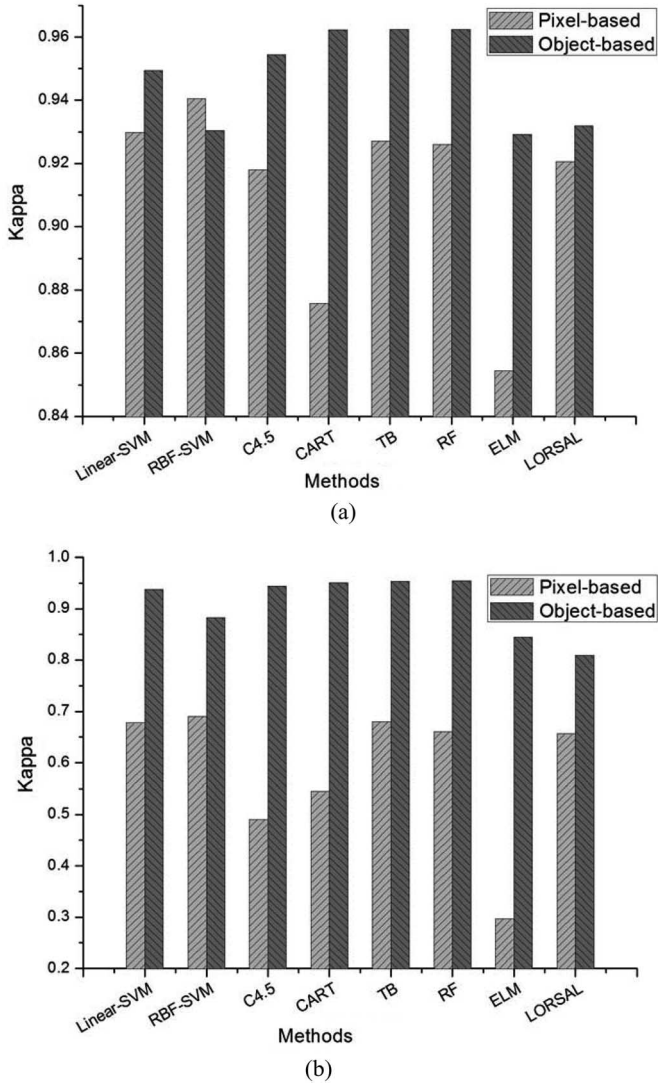


Fig. 13. Comparison of the accuracies between pixel-based and object-based water extractions for (a) Wuhan and (b) Shenzhen dataset, respectively.

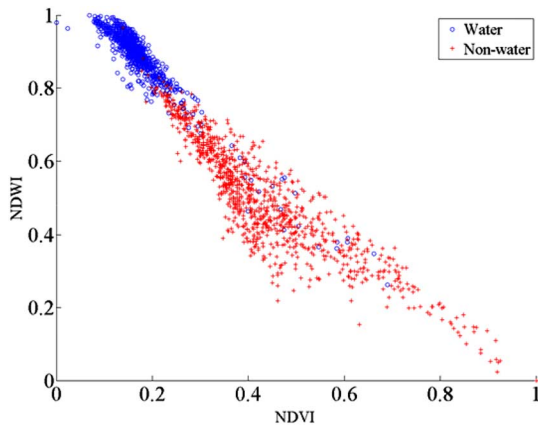


Fig. 14. Scatter plot of NDVI and NDWI, where 1000 samples per class (i.e., water and nonwater) are generated randomly from GeoEye-1 Wuhan dataset.

The imaging conditions (e.g., sun angle, sensor view angle, and cloud cover) also influence the accuracy of water detection. Specifically, in terms of sensor view angle, a small off-nadir

view angle is desirable for the water extraction and classification in urban areas. For instance, a tall building or tower in an image with a large off-nadir angle can shade the adjacent water surface. However, a low off-nadir angle can reduce the geometrical deformation of water areas. In fact, the nadir angles of images used in this study are not optimum, but the impact on the water detection is relatively small considering that the off-nadir angles for the two datasets (about 20°) are small.

The phenomenon of adjacency effect on the water is a common problem due to the atmospheric scattering [39]. Thus, the spectral reflectance of water bodies can be affected to some extent, especially in the boundary areas of water close to the bright features in urban areas. Santer and Schmechtig [40] discussed the adjacency effect on water surfaces by using the primary scattering approximation. The adjacency effect of the images used in the study is relatively small, and actually, the object-level feature description and classification can reduce the spectral difference and the adjacency effect for the water bodies.

In this paper, the thresholds for the information indexes (i.e., NDWI and NDVI) play an important role in the pixel-based water extraction. In general, a threshold can be selected by trial and error or using the peak-valley method of histogram segmentation [41]. At the pixel level, considering that the thresholding values are relatively stable in the experiments, the manually selected thresholds are used for the NDWI, NDVI, and MSI, for delineating water, vegetation, and shadow, respectively. Although the threshold scheme for water extraction can lead to a few uncertainties and errors, they can be effectively suppressed at the object level by considering the geometrical and textural attributes.

Last but not least, the training samples are usually delineated manually by visual inspection, but the sampling method is time-consuming. Thus, in future, further work will refer to more smart sampling strategy for the water extraction and classification. For instance, the active learning [42] or semi-supervised learning [43] techniques can be taken into account for optimizing the sampling strategy and saving the cost of manual labeling.

VI. CONCLUSION

In this paper, a novel pixel-object double-level machine-learning framework is proposed for water extraction and water-type identification from optical high-resolution remotely sensed imagery over urban areas. The effectiveness of the proposed strategy has been validated based on GeoEye-1 Wuhan and WorldView-2 Shenzhen, both of which are typical Chinese mega cities which have different characteristics of urban water resources.

The notable advantages and the new results of the proposed method are summarized as follows.

- 1) A set of information indexes, NDVI, NDWI, MSI, are used in the pixel level for extracting water areas. The consideration of the shadow index (MSI) is able to significantly reduce the false alarms of shadow (Fig. 4), which is a main source of errors for urban water extraction from high-resolution imagery.

- 2) The water information obtained by the pixel level is used as a preliminary result for the subsequent water-type identification at the object level, where a series of object-based geometrical and textural features are employed for discrimination between various water types. Our experiments show that the object-based features, such as area length-to-width ratio, shape index, density, and homogeneity, are essential for water-type classification.
- 3) The dual-level configuration of the proposed framework is able to integrate the information extraction from both pixel and object levels, for water detection and classification, respectively. The water extraction at the pixel level can be viewed as a preprocessing of the subsequent classification, which actually provides a mask for filtering out most of other urban structures. Another effective setting for the proposed framework is that, at the object level, the shadow is also viewed as a class to further correct the misclassifications between water and shadow derived from the pixel level. Experimental results (Fig. 13) show that this processing is effective for removing the false alarms of shadow by considering the object-oriented features.
- 4) A series of machine-learning algorithms are adopted at both pixel and object levels for water detection and classification, respectively. These methods include both state-of-the-art, e.g., SVM, RF, decision-tree, and new methods which are recently introduced into remote sensing, e.g., ELM and LORSAL. Therefore, it can be said that the conclusion obtained in this paper is reasonable and meaningful. An interesting phenomenon is that the decision-tree methods, especially for the RF and TB, achieved the optimal results in terms of both quantitative accuracy scores and visual inspection, particularly significantly outperforming SVM and ELM. A sensible explanation is that the object-based geometrical and textural features are rather effective for discriminating between different water types (Figs. 8 and 10). Consequently, the decision-tree methods, which directly consider the original features or their combinations for classification, gave better results than the SVM, ELM, and LORSAL, which are based on more complex machine-learning mechanism.

The proposed pixel-object dual-level framework has the potential for water detection and type identification, which are essential parameters for urban water management and monitoring. In future, we plan to apply the proposed framework in other urban areas, and further automate the water information extraction.

ACKNOWLEDGMENT

The authors would like to thank the anonymous reviewers for their insightful suggestions, which significantly improved the quality of this paper.

REFERENCES

- [1] J. Niemczynowicz, "Urban hydrology and water management-present and future challenges," *Urban Water*, vol. 1, no. 1, pp. 1–14, Mar. 1999.
- [2] O. Varis and P. Vakkilainen, "China's 8 challenges to water resources management in the first quarter of the 21st century," *Geomorphology*, vol. 41, no. 2, pp. 93–104, Nov. 2001.
- [3] S. K. McFeeters, "The use of the normalized difference water index (NDWI) in the delineation of open water features," *Int. J. Remote Sens.*, vol. 17, no. 7, pp. 1425–1432, Jan. 1996.
- [4] H. Q. Xu, "Modification of normalised difference water index (NDWI) to enhance open water features in remotely sensed imagery," *Int. J. Remote Sens.*, vol. 27, no. 14, pp. 3025–3033, Jul. 2006.
- [5] M. Bochow *et al.*, "On the use of airborne imaging spectroscopy data for the automatic detection and delineation of surface water bodies," in *Remote Sensing of Planet Earth*, Y. Chemin, Ed. Rijeka, Croatia: InTech, 2012, pp. 3–22.
- [6] G. L. Feyisa, H. Meilby, R. Fensholt, and S. R. Proud, "Automated water extraction index: A new technique for surface water mapping using Landsat imagery," *Remote Sens. Environ.*, vol. 140, pp. 23–35, Jan. 2014.
- [7] Z. L. Jiang, J. G. Qi, S. L. Su, Z. H. Zhang, and J. P. Wu, "Water body delineation using index composition and HIS transformation," *Int. J. Remote Sens.*, vol. 33, no. 11, pp. 3402–3421, Nov. 2012.
- [8] J.-F. Pekel *et al.*, "Development and application of multi-temporal colorimetric transformation to monitor vegetation in the desert locust habitat," *IEEE J. Sel. Topics Appl. Earth Observ. Remote Sens.* vol. 4, no. 2, pp. 318–326, Aug. 2011.
- [9] B. Sun, P. Zhao, L. Cheng, and X. Zhang, "Study on extraction method of water body from TM based on Munsell HSV transformation," *Remote Sens. Technol. Appl.*, vol. 24, no. 6, pp. 797–800, Dec. 2009.
- [10] D. D. Nguyen, "Water body extraction from multi spectral image by spectral pattern analysis," *ISPRS Int. Arch. Photogramm. Remote Sens. Spatial Inf. Sci.*, vol. 39-B8, pp. 181–186, Jul. 2012.
- [11] M. V. Shah, M. A. Choudhary, and K. Tewari, "River extraction from satellite image," *Int. J. Comput. Sci. Issues (IJCSI)*, vol. 8, no. 4, pp. 386–391, Jul. 2011.
- [12] J. Fu, J. Wang, and J. Li, "Study on the automatic extraction of water body from TM image using decision tree algorithm," in *Proc. SPIE 6625 Int. Symp. Photoelectron. Detect. Imag. 2007 Relat. Technol. Appl.*, 2008, vol. 6625, pp. 662502–662509.
- [13] C. Chen, J. Chen, X. Li, Q. Zhang, and S. Zheng, "Study on water body information extraction from high resolution remote sensing image based on object-oriented method," *Yellow River*, vol. 35, no. 9, pp. 68–70+73, Sep. 2013.
- [14] C. Li, G. Zhang, and L. Shen, "Water body extraction from remote sensing image based on AdaBoost algorithm," *Sci. Surv. Mapping*, vol. 38, no. 2, pp. 104–105, May 2013.
- [15] Y. Zhou, J. Luo, Z. Shen, X. Cheng, and X. Hu, "Adaptive extraction of water in urban areas based on local iteration using high-resolution multi-spectral image," in *Proc. IEEE Int. Geosci. Remote Sens. Symp. (IGARSS)*, Munich, Germany, 2012, pp. 6024–6027.
- [16] M. S. Mondal *et al.*, "Water area extraction using geocoded high resolution imagery of TerraSAR-X radar satellite in cloud prone Brahmaputra river valley," *J. Geomatics*, vol. 3, no. 1, pp. 9–12, Apr. 2009.
- [17] S. Klemenjak, B. Waske, S. Valero, and J. Chanussot, "Automatic detection of rivers in high-resolution SAR data," *IEEE J. Sel. Topics Appl. Earth Observ. Remote Sens.*, vol. 5, no. 5, pp. 1364–1372, Oct. 2012.
- [18] *Content and Index for the National Geographical Information Survey* [Online]. Available: <http://www.nmgch.gov.cn/xzzx/GDPJ012013.pdf>, accessed on Sep. 2014, In Chinese.
- [19] X. Huang and L. P. Zhang, "Morphological building/shadow index for building extraction from high-resolution imagery over urban areas," *IEEE J. Sel. Topics Appl. Earth Observ. Remote Sens.*, vol. 5, no. 1, pp. 161–172, Feb. 2012.
- [20] C. J. Tucker, "Red and photographic infrared linear combinations for monitoring vegetation," *Remote Sens. Environ.*, vol. 8, no. 2, pp. 127–150, May 1979.
- [21] X. Huang and L. P. Zhang, "A multidirectional and multiscale morphological index for automatic building extraction from multispectral GeoEye-1 imagery," *Photogramm. Eng. Remote Sens.*, vol. 77, no. 7, pp. 721–732, Jul. 2011.
- [22] L. Bruzzone, F. Roli, and S. B. Serpico, "An extension of the Jeffreys–Matusita distance to multiclass cases for feature selection," *IEEE Trans. Geosci. Remote Sens.*, vol. 33, no. 6, pp. 1318–1321, Nov. 1995.
- [23] R. M. Iaralick, K. Shanmugan, and I. Dinstein, "Textural features for image classification," *IEEE Trans. Syst. Man Cybern.*, vol. 3, no. 6, pp. 610–621, Nov. 1973.
- [24] O. Chapelle, P. Haffner, and V. N. Vapnik, "Support vector machines for histogram-based image classification," *IEEE Trans. Neural Netw.*, vol. 10, no. 5, pp. 1055–1064, Sep. 1999.
- [25] F. Melgani and L. Bruzzone, "Classification of hyperspectral remote sensing images with support vector machines," *IEEE Trans. Geosci. Remote Sens.*, vol. 42, no. 8, pp. 1778–1790, Aug. 2004.

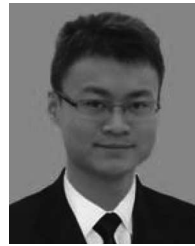
- [26] G. Huang, Q. Zhu, and C. Siew, "Extreme learning machine: Theory and applications," *Neurocomputing*, vol. 70, no. 1, pp. 489–501, May 2006.
- [27] Y. Zhou, J. Peng, and C. Chen, "Extreme learning machine with composite kernels for hyperspectral image classification," *IEEE J. Sel. Topics Appl. Earth Observ. Remote Sens.*, 2014, doi: 10.1109/JSTARS.2014.2359965, to be published.
- [28] L. Breiman, "Bagging predictors," *Mach. Learn.*, vol. 24, no. 2, pp. 123–140, 1996.
- [29] L. Rokach and O. Maimon, "Top-down induction of decision trees classifiers—A survey," *IEEE Trans. Syst. Man Cybern. Appl. Rev.*, vol. 35, no. 4, pp. 476–487, Nov. 2005.
- [30] J. R. Quinlan, "Induction of decision trees," *Mach. Learn.*, vol. 1, no. 1, pp. 81–106, Mar. 1986.
- [31] S. L. Salzberg, "C4.5: Programs for machine learning by J. Ross Quinlan. Morgan Kaufmann Publishers, Inc., 1993," *Mach. Learn.*, vol. 16, no. 3, pp. 235–240, Sep. 1994.
- [32] L. Olshen and C. J. Stone, *Classification and Regression Trees*. Belmont, CA, USA: Wadsworth, 1984.
- [33] T. K. Ho, "The random subspace method for constructing decision forests," *IEEE Trans. Pattern Anal. Mach. Intell.*, vol. 20, no. 8, pp. 832–844, Aug. 1998.
- [34] T. Shi and S. Horvath, "Unsupervised learning with random forest predictors," *J. Comput. Graph. Statist.*, vol. 15, no. 1, pp. 118–138, Mar. 2006.
- [35] J. Bioucas-Dias and M. Figueiredo, "Logistic regression via variable splitting and augmented Lagrangian tools," Instituto Superior Técnico, TULisbon, Lisbon, Portugal, Tech. Rep., 2009.
- [36] X. Huang *et al.*, "Multiple morphological profiles from multicomponent-base images for hyperspectral image classification," *IEEE J. Sel. Topics Appl. Earth Observ. Remote Sens.*, vol. 7, no. 12, pp. 4653–4669, Dec. 2014.
- [37] J. Li, J. Bioucas-Dias, and A. Plaza, "Hyperspectral image segmentation using a new Bayesian approach with active learning," *IEEE Trans. Geosci. Remote Sens.*, vol. 49, no. 10, pp. 3947–3960, Oct. 2011.
- [38] D. M. Powers, "Evaluation: From precision, recall and F-measure to ROC, informedness, markedness and correlation," *J. Mach. Learn. Technol.*, vol. 2, no. 1, pp. 37–63, Dec. 2011.
- [39] D. Tanré, P. Y. Deschamps, P. Duhaut, and M. Herman, "Adjacency effect produced by the atmospheric scattering in thematic mapper data," *J. Geophys. Res. Atmos. (1984–2012)*, vol. 92, no. D10, pp. 12000–12006, 1987.
- [40] R. Santer and C. Schmechtig, "Adjacency effects on water surfaces: Primary scattering approximation and sensitivity study," *Appl. Opt.*, vol. 39, no. 3, pp. 361–375, 2000.
- [41] J. Delon, A. Desolneux, J. L. Lisani, and A. B. Petro, "A nonparametric approach for histogram segmentation," *IEEE Trans. Image Process.*, vol. 16, no. 1, pp. 253–261, Jan. 2007.
- [42] D. Tuia, F. Ratle, F. Pacifici, M. F. Kanevski, and W. J. Emery, "Active learning methods for remote sensing image classification," *IEEE Trans. Geosci. Remote Sens.*, vol. 47, no. 7, pp. 2218–2232, Jul. 2009.
- [43] L. Bruzzone, C. Mingmin, and M. Marconcini, "A novel transductive SVM for semisupervised classification of remote-sensing images," *IEEE Trans. Geosci. Remote Sens.*, vol. 44, no. 11, pp. 3363–3373, Nov. 2006.



Xin Huang (M'13–SM'14) received the Ph.D. degree in photogrammetry and remote sensing from Wuhan University, Wuhan, China, in 2009.

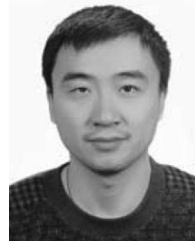
He is working with the State Key Laboratory of Information Engineering in Surveying, Mapping, and Remote Sensing (LIESMARS). Since 2012, he has been a Full Professor with LIESMARS, Wuhan University. He has authored more than 60 peer-reviewed articles in the international journals. His research interests include hyperspectral data analysis, high-resolution image processing, pattern recognition, and remote-sensing applications.

Dr. Huang was the recipient of the Top-Ten Academic Star of Wuhan University in 2009, the Boeing Award for the Best Paper in Image Analysis and Interpretation from the American Society for Photogrammetry and Remote Sensing in 2010, the New Century Excellent Talents in University from the Ministry of Education of China in 2011, and the National Excellent Doctoral Dissertation Award of China in 2012. In 2011, he was recognized by the IEEE Geoscience and Remote Sensing Society (GRSS) as the Best Reviewer of IEEE GEOSCIENCE AND REMOTE SENSING LETTERS. He was the winner of the IEEE GRSS 2014 Data Fusion Contest. Since 2014, he serves as an Associate Editor of the IEEE GEOSCIENCE AND REMOTE SENSING LETTERS.



Cong Xie received the B.S. degree in surveying engineering from the School of Geodesy and Geomatics, Wuhan University, Wuhan, China, in 2014. He is currently pursuing the M.S. degree in photogrammetry and remote sensing.

He is currently with the State Key Laboratory of Information Engineering in Surveying, Mapping, and Remote Sensing, Wuhan University. His research interests include image processing, machine learning, and water detection from remotely sensed images.



Xing Fang received the Bachelor's degree in photogrammetry and remote sensing from Wuhan University, Wuhan, China, in 2004, and the Ph.D. degree in geodetic science from Leibniz University of Hanover, Hanover, Germany, in 2011.

He is currently an Associate Professor with the School of Geodesy and Geomatics, Wuhan University. He has authored eight peer-reviewed articles in the international journals. His research interests include data analysis, high-dimensional data processing, pattern recognition, and geodetic

applications.

Dr. Fang was the recipient of the Chutian Scholar of Hubei Province in 2011.



Liangpei Zhang (M'06–SM'08) received the B.S. degree in physics from Hunan Normal University, Changsha, China, in 1982, the M.S. degree in optics from Chinese Academy of Sciences, Xian, China, in 1988, and the Ph.D. degree in photogrammetry and remote sensing from Wuhan University, Wuhan, China, in 1998.

He is currently the Head of the Remote Sensing Division, State Key Laboratory of Information Engineering in Surveying, Mapping, and Remote Sensing, Wuhan University. He is also a Chang-Jiang Scholar Chair Professor appointed by the Ministry of Education of China. He is currently a Principal Scientist for the China State Key Basic Research Project (2011–2016) appointed by the Ministry of National Science and Technology of China to lead the remote sensing program in China. He has authored more than 300 research papers. He is the holder of five patents. His research interests include hyperspectral remote sensing, high-resolution remote sensing, image processing, and artificial intelligence.

Dr. Zhang is a Fellow of the Institution of Engineering and Technology, an Executive Member (Board of Governor) of the China National Committee of the International Geosphere-Biosphere Programme, and an Executive Member of the China Society of Image and Graphics. He regularly serves as a Co-Chair of the series SPIE Conferences on Multispectral Image Processing and Pattern Recognition, Conference on Asia Remote Sensing, and many other conferences. He edits several conference proceedings, issues, and Geoinformatics symposiums. He also serves as an Associate Editor of the *International Journal of Ambient Computing and Intelligence*, the *International Journal of Digital Multimedia Broadcasting*, the *Journal of Geospatial Information Science*, the *Journal of Remote Sensing*, and the IEEE TRANSACTIONS ON GEOSCIENCE AND REMOTE SENSING.